25th ABCM International Congress of Mechanical Engineering
October 20-25, 2019, Uberlândia, MG, Brazil

COB-2019-0176
BENDING AND TORSION FATIGUE ANALYSES OF CRANKSHAFTS

Ferreira, R. N.
Bittencourt, M. L.
Univesity of Campinas, UNICAMP.
Rua Mendeleyev, 200, Campinas-SP
nascimento.cps@gmail.com
mlb@fem.unicamp.br.

Abstract. *The intensive search for optimized projects with lower production costs influenced by the global competition context has encouraged the development of lighter and more efficient combustion engines. The reduction of mass in engine crankshafts may have a significant impact on the performance of new engines. However, crankshafts have complex geometries and are subjected to high dynamic loads which are critical for fatigue failure. Furthermore, crankshafts always require caution in the design phases since any failure in operation could lead to catastrophic accidents. For this reason, new crankshaft models ought to be assessed and approved in standards to guarantee infinite life in fatigue. At this work a bending and a torsion resonant test rigs were designed and manufactured to evaluate the fatigue life of a commercial crankshaft model. Static structural numerical analyses were carried out to determine the stress distribution and critical areas for bending and torsion loads. Both bending and torsion test rigs presented good performance for fatigue testing and congruency with numerical analyses. The results obtained in this work cover broadly the fatigue phenomena in crankshafts for bending and torsion loads and can be used as base for the development of new crankshaft models.*

Keywords: *Crankshaft, Engine, Fatigue, Finite elements, vibration.*

1. INTRODUCTION

In internal combustion engines, crankshafts convert the energy from linear motion of pistons into torque for the mechanical coupled system. Crankshafts are usually made of cast iron or forged steel and have complex geometry with high stress concentration in the fillets. While in operation, it is subjected to high dynamic bending and torsion loads. Crankshafts ought to be designed with infinite fatigue life and well balanced so that the vibration and noise in the internal combustion engine is the smallest possible. A schematic drawing of a four-cylinder engine crankshaft is illustrated in Fig 1.

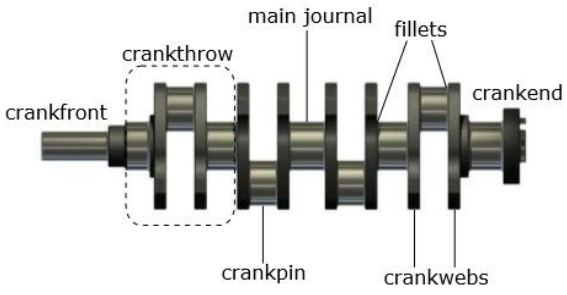

Figure 1. Schematic drawing of a four-cylinder crankshaft
Available from: (Morais, 2017).

.

Fatigue failure in crankshafts is a usual problem in the automotive field. Every crankshaft model designed is cautiously assessed and approved according to severe standards. The resonant test method is the most reliable technique used for fatigue test in the automotive industry (Chien et al., 2005; Spiteri et al., 2005; Villalva and Junior 2010). This method is based on the principle of frequency shift with crack propagation in the materials. Gudmundson (1982) showed mathematically that the eigen frequency of a component changes with crack propagation. Feng and Li (2003)

used this principle to develop an automated controlling system to detect frequency shift and drive the specimens in the resonant frequency. This paper (Feng and Li, 2003) also showed that the moment applied in the tested system can be determined only by acceleration. Feng and Li (2003) still proposed static and dynamic calibrations using strain as intermediate quantity. In the static calibration, a relation is obtained between moment and strain by accurate measures. The dynamic calibration, otherwise, relates the acceleration and strain quantities for different amplitudes of excitation. Therefore, it is possible to control the moment applied in the specimens tracking the acceleration of the harmonic response. Figure 2 summarizes the relation between static and dynamic calibration.

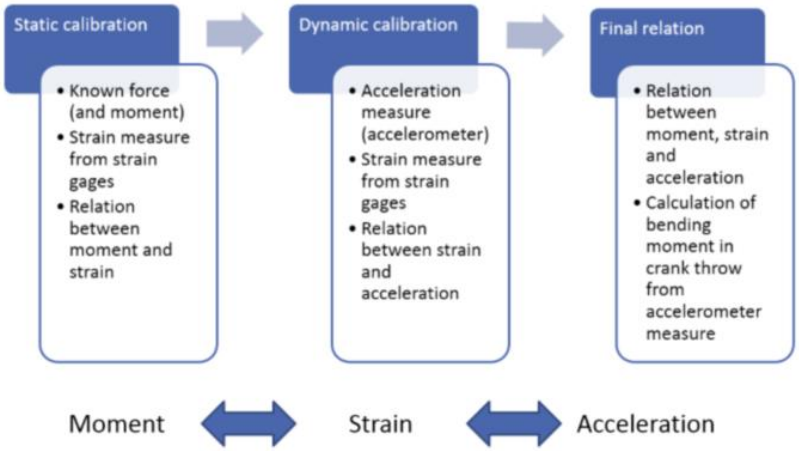

Figure 2. Relation between static and dynamic calibration procedures.
Available from: (Morais, 2017).

Spiteri et al. (2005) studied the frequency shift criterion for failure mode of cast iron crankshaft. Them (Spiteri et al., 2005) determined the endurance limit for V6 and V8 crankshafts using the staircase statistical method and monitoring cracks and resonance shift in the specimens. This paper (Spiteri et al., 2005) concluded that 3% decrease in frequency would capture 90% of a two-piece failure.

Due to the large production scale, crankshaft is theme for many studies in the automotive field. Most of these studies are focus on the fillet radii subject to deep rolling treatment and fatigue failure caused by bending loading. The bending fatigue occurs in most cases for gasoline engines; however, torsion fatigue may also appear, especially for diesel engines (Fonseca, 2015). There is little information brought out about torsion fatigue tests. Villalva (2010) carried out simulations for both bending and torsion loading and obtained good correlation with strain gauges measurements. Feng and Li (2003) covered briefly about torsion test rigs characteristics and verified that, in torsion loading, the crack nucleation may initiate in the oil holes with orientation of 45 degrees to the longitudinal direction of the crankpin.

The crankshaft assessed in this work was supplied by an international automotive company. The specimens were obtained from a forged four-stroke crankshaft manufactured with nodular cast iron material. Its mean material properties obtained by Morais (2017) are indicated in the Tab.1. Figure 3 show the 3D geometry of the crankshaft assessed in this paper.

Figure 3. Crankthrow and crankshaft 3D geometries.

Table 1. Material properties of the crankshaft

Young modulus [GPa]	Yield stress [MPa]	Ultimate stress [MPa]	Poisson coefficient
177.67	400	708.11	0.275

2. EXPERIMENTAL FATIGUE ANALYSIS

The evaluation of fatigue life in crankshafts requires application of intense bending and torsion loading. At this work, fatigue test rigs were designed and manufactured to apply loads in resonant modes of vibration. It consists of two inertia plates and two pairs of sleeves fixing the crankthrow. While the bending test rig is suspended by wires, the torsion one is suspended by fixed supports with bearings. In both cases, the inertia plates are driven by an electrodynamic shaker controlled by a signal generator. The complete test setup scheme used in the fatigue testing is shown in the Fig. 4.

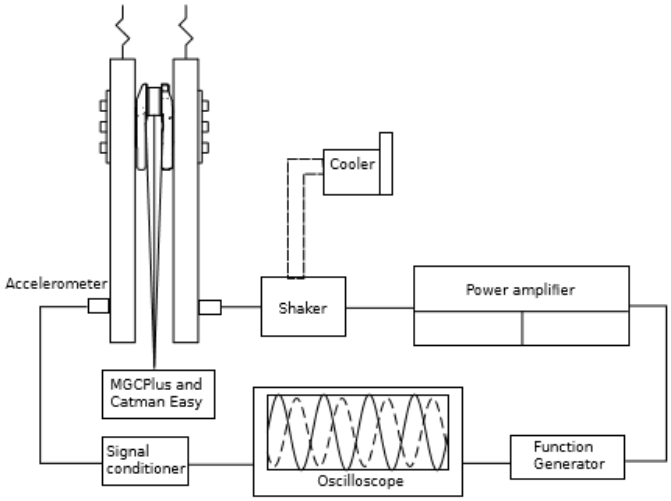

Figure 4. Complete dynamic test setup scheme.
Available from: (Morais, 2017).

For both bending and torsion testing set up, the signal from an accelerometer positioned in the inertia plate and the strain gages placed in the crankpin were read by a data acquisition system. The resulting stress was computed and related to the acceleration after a dynamic calibration. A relation between moment and strain was also obtained in a static calibration. Afterwards, the fatigue testing was carried out according to the staircase method with a failure criterion of 3% decrease in the resonance frequency. The torsion and bending test rigs are given in Fig. 5.

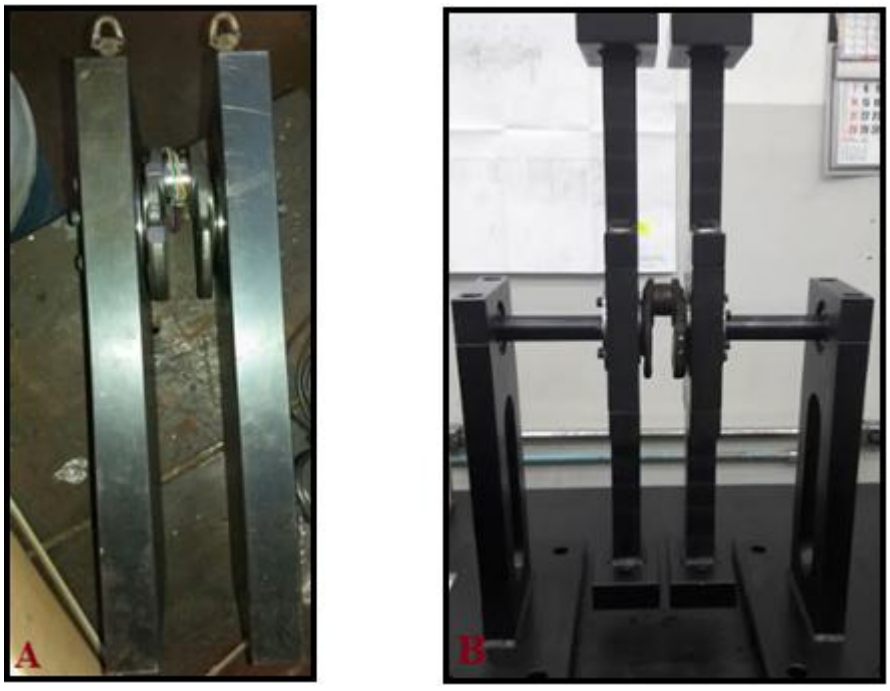

Figure 5. (A) Bending and (B) torsion test rig.

2.1 Static Calibration

In the static calibration procedure, an increasing load was applied in the inertial plates in such a way that the specimen was subjected to bending or torsion loading. In this paper, the different loads applied to the specimens were read by a load cell of HBM U10M 25kN model. For the bending case, a KYOWA KFG-3-120-C1-11 3 mm gauge was used to measure strain in the center bottom of the crankpin. The following relation was used to compute the stresses:

$$\sigma = \frac{E}{(1-\nu^2)}\varepsilon \tag{1}$$

where σ is the stress, ε is the measured strain, E is the Young modulus and ν is the Poisson coefficient for the cast iron taken from Tab. 1.

The bending test rig was positioned according to Fig. 6b) and the force was applied by a hydraulic jack. The static calibration was also simulated on Ansys in a static structural analysis by finite element (FE) method. Figure 6a) shows the constrains used to compute the equivalent Von-Mises stress for the simulated system.

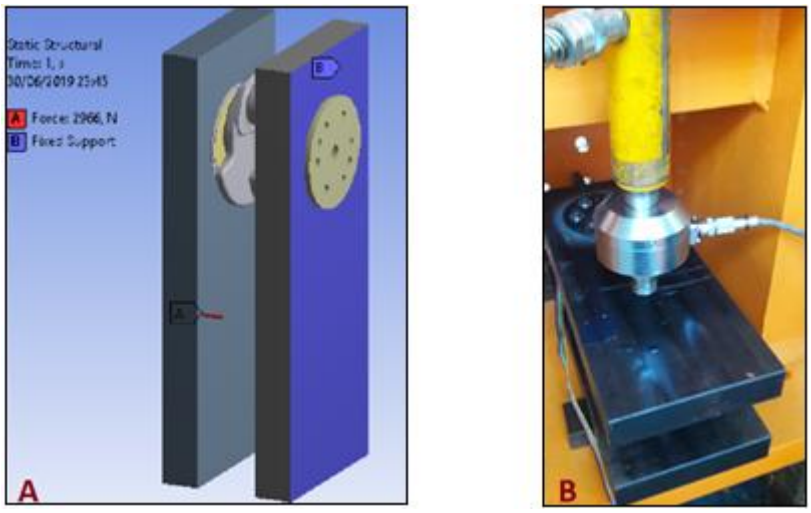

Figure 6. (A) Constrains of the FE analysis and (B) experimental set up for bending static calibration.

For both experimental and FE analyses, the force was applied in the unconstrained inertial plate with arm length of 236 mm from the crankpin center axis. The Von-Mises stress distribution for bending moment of 700 Nm is shown in the Fig. 7a). Figure 7b) shows the static calibration chart for the numerical and experimental test.

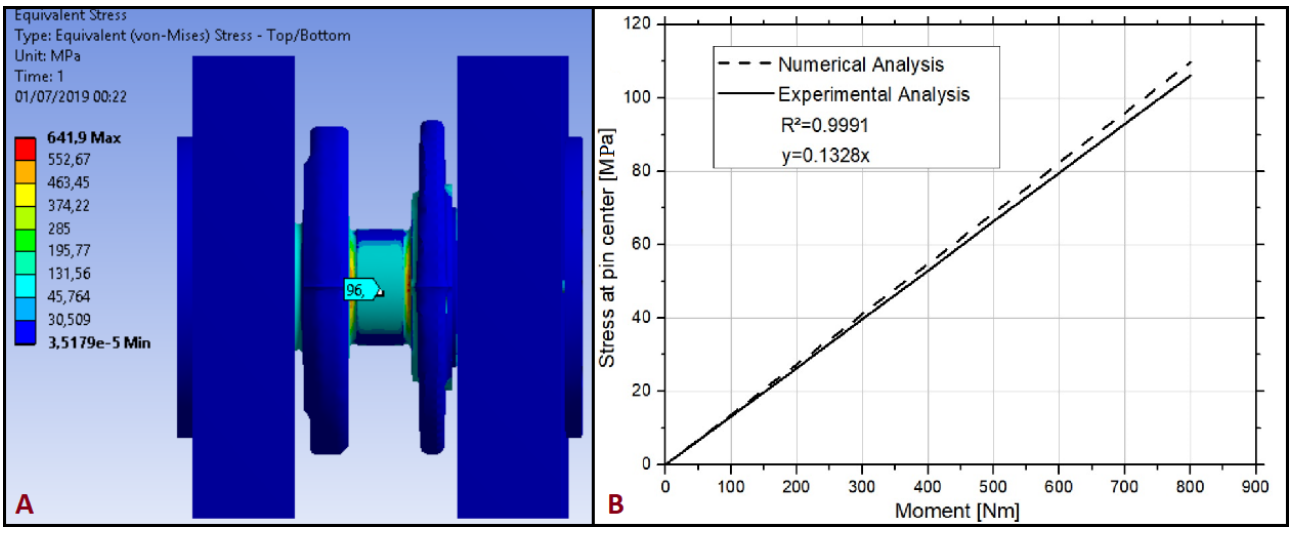

Figure 7. (A) Equivalent stress distribution from bending numerical analysis and (B) chart of numerical and experimental static calibration for the bending loading.

In the torsion static calibration case, the torsion test rig was positioned according to Fig. 8b). The force was applied in the bottom left arm while the bottom right one was fixed with a support. A KYOWA KFG-3-120-D17-11 gauge was placed on the top of the crankpin and the principal stresses were computed by the following equations:

$$\sigma_1 = \frac{E}{(1-\nu^2)}(\varepsilon_1 + \nu\varepsilon_2) \tag{2}$$

$$\sigma_2 = \frac{E}{(1-\nu^2)}(\varepsilon_2 + \nu\varepsilon_1) \tag{3}$$

where σ_1 and σ_2 are the principal stresses and ε_1 and ε_2 are the strains measured in the principal directions. The principal stresses were used to compute the equivalent stress for each moment applied to the crankthrow. Equation (4) was used to compute the resulting equivalent stress (σ_v):

$$\sigma_v = \sqrt{\sigma_1^2 - \sigma_1\sigma_2 + \sigma_2^2} \tag{4}$$

The finite element method was also used to simulate the static calibration for the torsion loading case. The constrains used in the simulation are indicated in the Fig. 8a). The arm length from applied force point till main journal center axis is 350 mm.

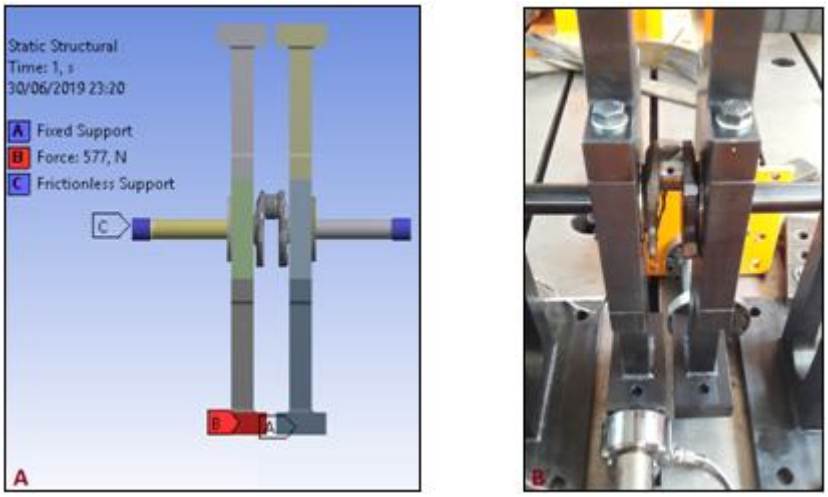

Figure 8. (A) Constrains of the FE analysis and (B) experimental set up for torsion static calibration.

Figure 9 a) shows the equivalent stress distribution in the crankthrow loaded by torque of 202 Nm. A comparison between the numerical and experimental curve for the torsion case is illustrated in the chart from Fig. 9b).

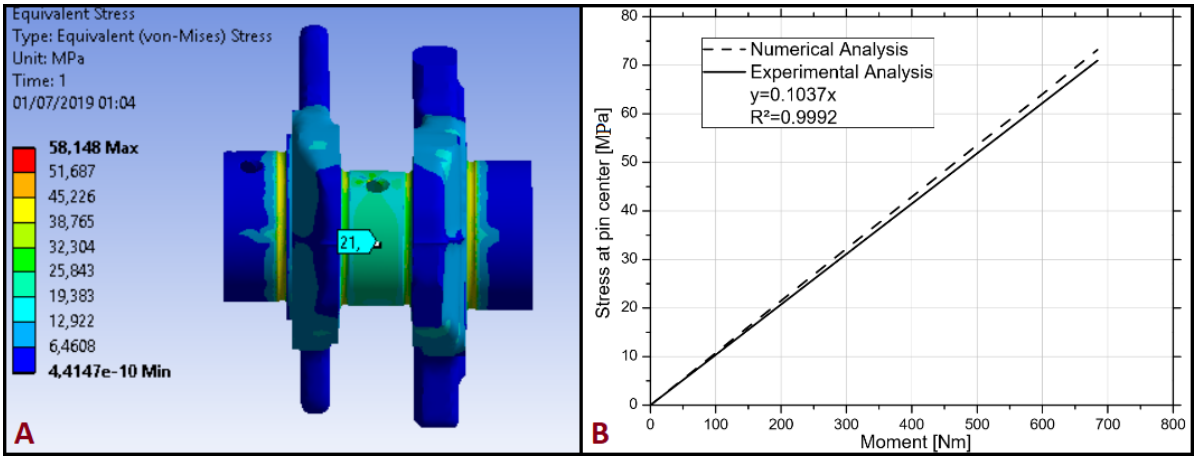

Figure 9. (A) Equivalent stress distribution from torsion numerical analysis and (B) chart of numerical and experimental static calibration for the torsion loading case.

2.2 Dynamic Calibration

In the dynamic calibration procedure, an accelerometer was positioned in the inertial plates and the system was driven by an electrodynamic shaker in the resonant frequency. It was used a Modal Shop 2100E11 electrodynamic shaker with 440 N peak force and 1in stroke. The resonant frequency was around 70 Hz for both bending and torsion test rigs. The same strain gauges positioning from static calibration were used to perform the dynamic one. The amplitude of excitation was increased from zero until 10 g and the acceleration was correlated to the strain measures. Equation (1) was used to compute stress in the bottom center of the crankpin in the bending mode of vibration. Figure 10b) shows the resulting curve from the bending dynamic calibration.

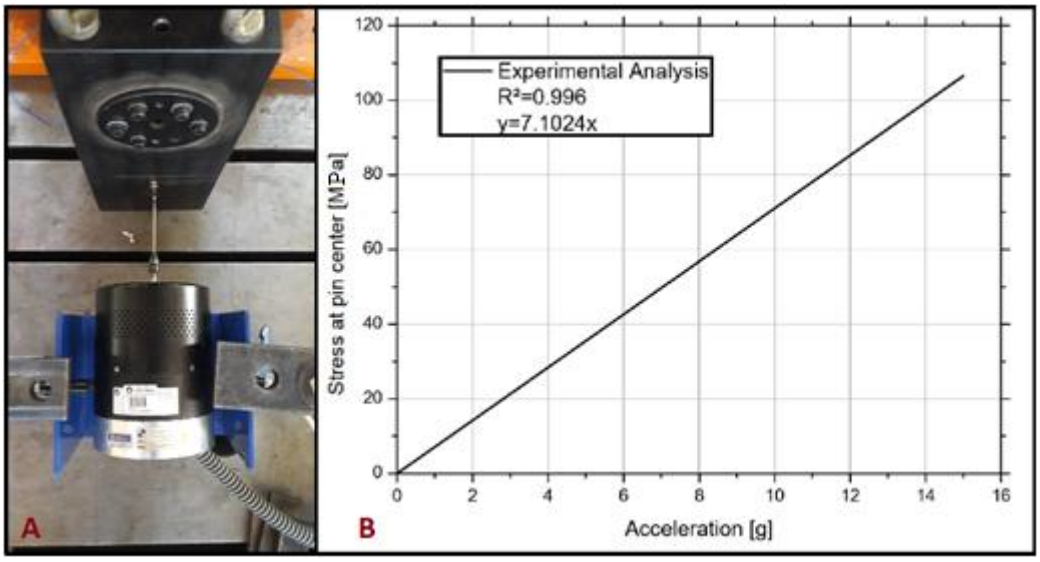

Figure 10. (A) Experimental set up and (B) experimental curve for bending dynamic calibration.

In the torsion test rig, one accelerometer was placed in each bottom arm to guarantee the system was operating in the torsion mode of vibration. Therefore, the signal from the accelerometers was lagged by 180º. Equation (2), (3) and (4) were used to compute the equivalent stress in the top center of the crankpin. Figure 11b) shows the resulting curve from torsion dynamic calibration.

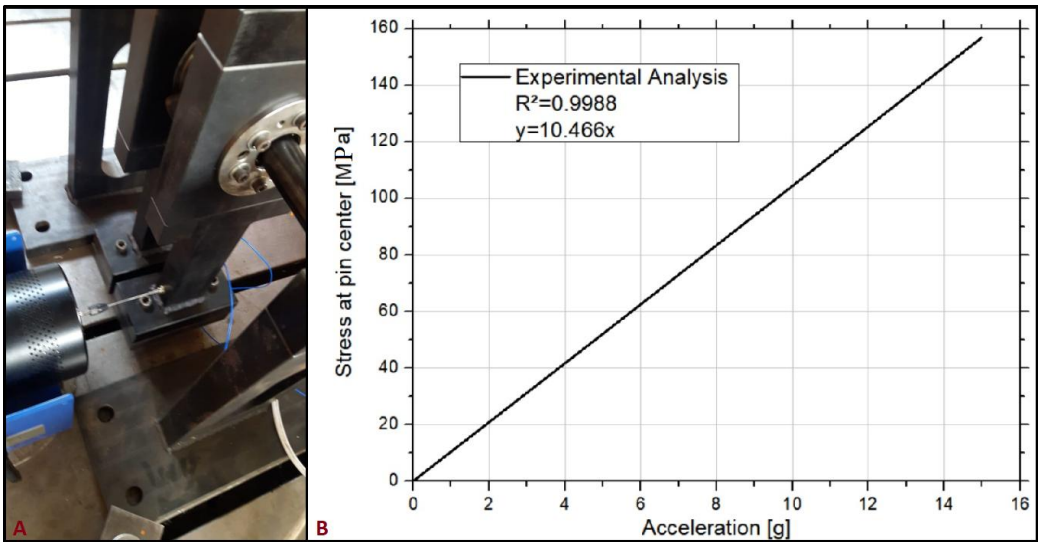

Figure 11. (A) Experimental set up and (B) experimental curve for torsion dynamic calibration.

After the static and dynamic calibration procedures, it was possible to obtain a direct relation between acceleration and the moment applied in the specimens. These results were used to controll the fatigue tests and determine the fatigue limit for bending and torsion loading.

2.3 Fatigue analyses

In order to determine the mean fatigue limit from staircase method, it was used the Dixon-Mood (1948) approach as data reduction technique. The mean fatigue limit was computed in function of the moment applied to the specimens. The equations used in the Dixon-Mood method were based on (Lee, 2005). The mean fatigue limit was calculated by the following equation:

$$\mu = M_0 + d\left(\frac{A}{\sum n_i} \mp \frac{1}{2}\right) \tag{5}$$

where, μ is the mean fatigue limit, d is the constant step adopted in the staircase method, M_0 is the lowest moment applied to the specimens and n_i.is the number of the less frequent event at load level i. The signal "-"in the Eq. (6) is used if the less frequent event is "failure" and the signal "+" is used if the less frequent event is "suspension". The quantity denoted by A can be calculated by Eq. (6)

$$A = \sum i n_i \tag{6}$$

The staircase chart for the bending fatigue case is represented in Figure 12. For this case, the less frequent event can be either failure or suspension since both occurred four times. In this work it was chosen failure as less frequent event for the bending mean fatigue calculation. Table 2 summarizes the number of failures and bending moments for each load level.

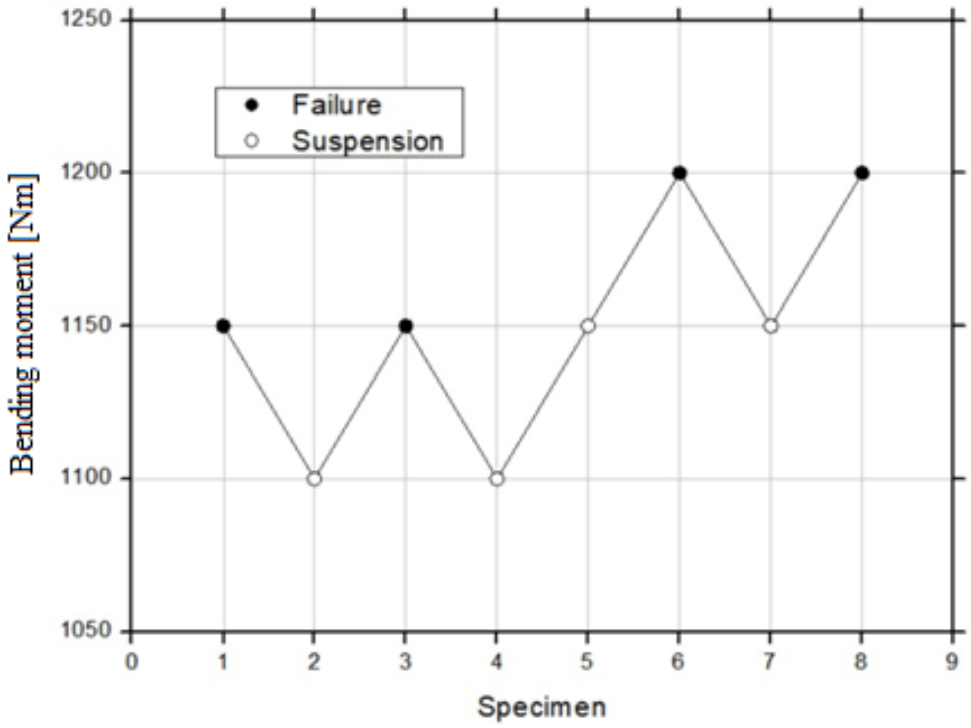

Figure 12. Visual representation of the staircase data for bending fatigue test.

Table 2. Load levels and occurrences for bending staircase data reduction.

Bending moment M_i [Nm]	Load level number i	Number of occurrences n_i
1100	0	0
1150	1	2
1200	2	2

Figure 13 show the staircase chart for the torsion fatigue case. Both failure and suspension events occurred three times, so any event could be used to calculate the mean fatigue limit for this case. Table 3 contains the values of torsion moment and number of failures for each load level.

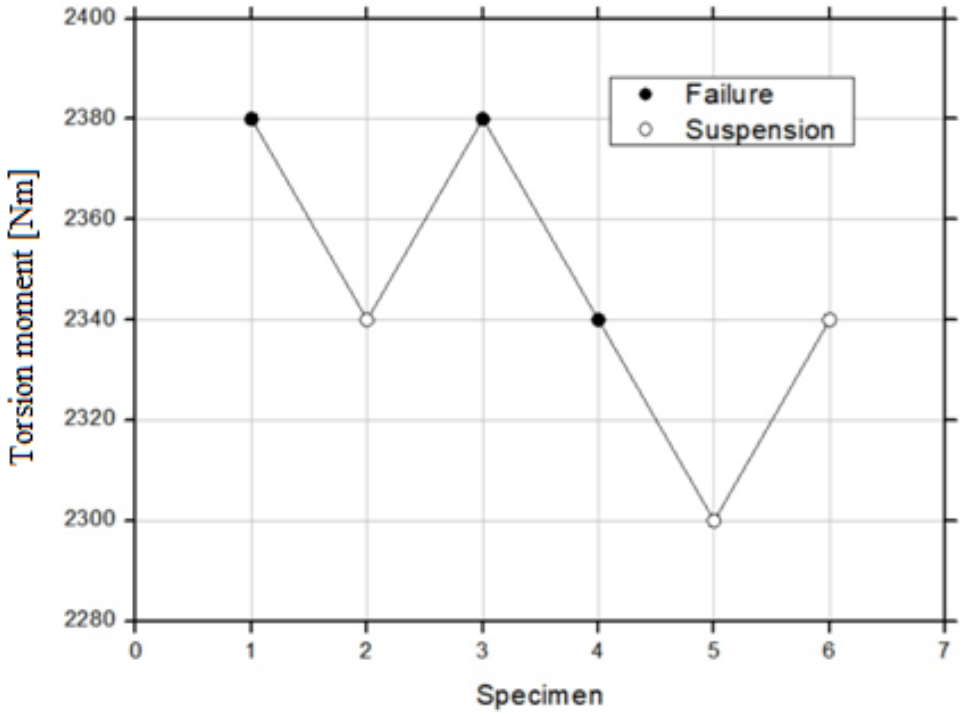

Figure 13. Visual representation of the staircase data for the torsion fatigue test.

Table 3. Load levels and occurrences for torsion staircase data reduction.

torsion moment M_i [Nm]	Load level number i	Number of occurrences n_i
2300	0	0
2340	1	1
2380	2	2

Equations (5) and (6) were used considering the data from Tab. 2 and 3 to calculate the mean fatigue limit for 2 million cycles. These results are summarized in the Tab.4:

Table 4. Mean fatigue limit calculation.

Fatigue test	A	M_0 [Nm]	d [Nm]	$\sum n_i$	μ [Nm]
Bending	6	1100	50	4	1150
Torsion	5	2300	40	3	2347

The fatigue test indicated that crankshafts are more sensitive to bending than torsion loads due to high stress concentration in the fillets. Even after deep rolling treatment, the fatigue limit for torsion loading (2347 Nm) is twice as much as bending one (1150 Nm). The liquid penetrant testing indicated cracks in the fillet radii in the failed specimens subjected to bending moment. The failed specimens from the torsion case, however, had crack nucleation in the oil holes. No crack was found in the specimens that survived the 2 million cycles without resonant frequency shift. Figure 14 and 15 show the comparison between the critical region pointed by finite element simulations and the cracks propagated in the bending and torsion specimens, respectively.

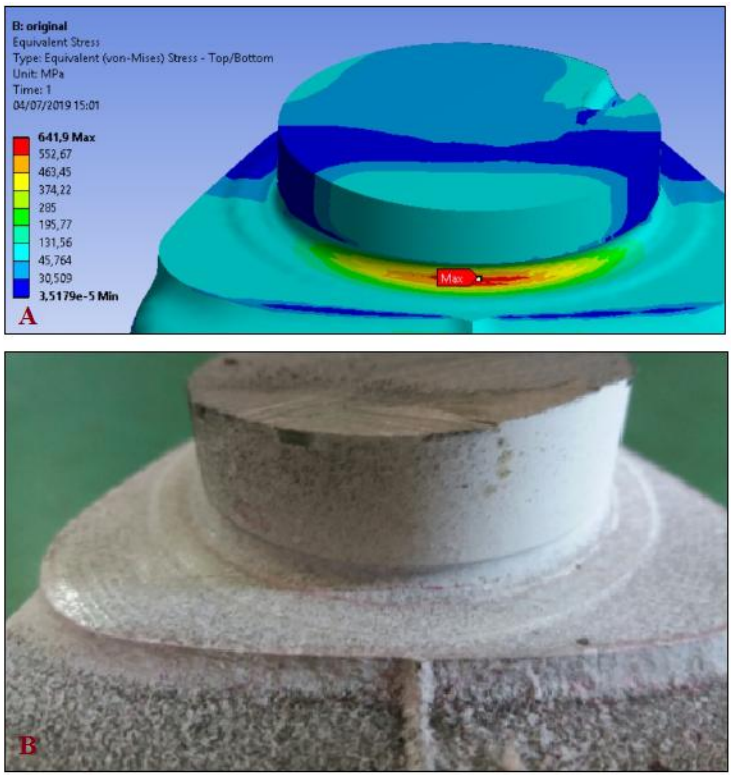

Figure 14. (A) Critical area in the fillet radii pointed by FE analysis and (B) crack revealed by liquid penetrant testing in the bending specimens.
Modified from: (Morais, 2017).

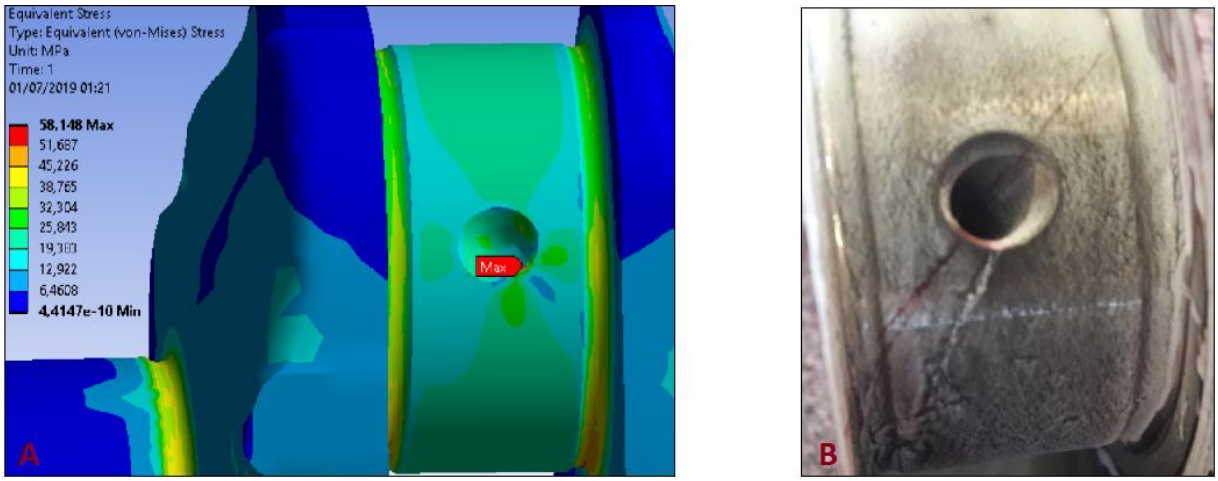

Figure 15. (A) Critical area in the oil hole pointed by FE analysis and (B) crack revealed by liquid penetrant testing in the torsion specimens.

3. CONCLUSION

This work was successful in assess the fatigue life of specimens tested for bending and torsion loading. The resonant testing method was shown very efficient and time saving for fatigue evaluation. At the same time, the 3% frequency shift criterion was able to detect cracks with precision. The static calibration simulated by finite elements successfully indicated the most critical areas for crack nucleation and presented good correlation with experimental results for both bending and torsion tests. The liquid penetrant analysis detected cracks in the specimens that had frequency decrease before 2 million cycles. The specimens that failed in the bending tests had crack nucleation in the crankpin fillet radii. In the torsion specimens, otherwise, the cracks nucleated in the crankpin oil hole. The bending fatigue limit (1150 Nm) was shown more critical than the torsion one (2347 Nm). This result is consistent with static analysis that indicted intense stress concentration in the fillet radii for bending moment.

4. REFERENCES

CHIEN, W. et al. Fatigue analysis of crankshaft sections under bending with consideration of residual stresses.InternationalJournalofFatigue, Elsevier, v. 27, n. 1, p. 1–19, 2005.

DIXON, W. J.; MOOD, A. M. A method for obtaining and analyzing sensitivity data. Journal of the American Statistical Association, Taylor & Francis, v. 43, n. 241, p. 109–126, 1948.

FENG, M.; LI, M. Development of a computerized electrodynamic resonant fatigue test machine and its applications to automotive components. SAE Technical Paper, 2003.

FONSECA, L. G. A. Crankshaft deep rolling modeling through explicit analysis using finite element method. Master's Thesis — Instituto Tecnológico de Aeronáutica, 2015.

GUDMUNDSON, P. Eigen frequency changes of structures due to cracks, notches or other geometrical changes. Journal of the Mechanics and Physics of Solids, Elsevier, v. 30, n. 5, p. 339–353, 1982.

LEE,Y.-L. Fatigue testing and analysis: theory and practice. [S.l.]: Butterworth-Heinemann, 2005. v. 13.

MORAES, E.B. Numerical and experimental fatigue analysis of crankshaft. 2017. Master thesis. Faculdade de Engenharia Mecânica, Universidade Estadual de Campinas, Campinas.

SPITERI, P. V.; LEE, Y.-L.; SEGAR, R. An exploration of failure modes in rolled, ductile, cast-iron crankshafts using a resonant bending testing rig. SAE Technical Paper, 2005.

VILLALVA, S. G.; JUNIOR, E. G. F. Correlation between cae and experimental fatigue bench tests for automotive crankshafts. SAE Technical Paper, 2010.